

Sliding wear of nanocrystalline Ni–W: Structural evolution and the apparent breakdown of Archard scaling

Timothy J. Rupert, Christopher A. Schuh *

Department of Materials Science and Engineering, Massachusetts Institute of Technology, 77 Massachusetts Avenue, Cambridge, MA 02139, USA

Received 2 March 2010; accepted 5 April 2010

Available online 7 May 2010

Abstract

Sliding wear of nanocrystalline Ni–W alloys with grain sizes of 3–47 nm, a range which spans the transition in deformation mechanisms from intra- to inter-granular, has been studied through pin-on-disk wear testing. The extreme conditions produced during sliding wear are found to result in structural evolution and a deviation from Archard scaling for the finest grain sizes; in the finest nanocrystalline materials wear resistance is higher than would be expected based on hardness alone. The repetitive sliding load is found to lead to a modest amount of grain growth and grain boundary relaxation, which in turn leads to local hardening in the wear track. Analysis of the dynamic microstructure suggests that it is produced primarily as a result of local plasticity and is not principally due to frictional heating.

© 2010 Acta Materialia Inc. Published by Elsevier Ltd. All rights reserved.

Keywords: Nanocrystalline materials; Wear; Mechanical properties; Ni–W alloys; Grain boundary migration

1. Introduction

Nanocrystalline metals (those with grain sizes below 100 nm) represent the extreme of grain refinement, garnering a great deal of attention for their promise of exceptional strength. In addition, the emergence of novel grain boundary-dominated deformation mechanisms such as grain boundary dislocation emission [1–3], grain boundary sliding [4,5], grain rotation [6–8], and grain boundary migration [9–11], has sparked a flurry of scientific interest. While a great deal of research on nanocrystalline materials has focused on basic mechanical properties such as yield strength and hardness, limited resources have been directed towards the evaluation of more complex mechanical behaviors, including abrasion and wear. For traditional engineering metals wear resistance can often be related simply to hardness through the Archard equation, which states

that the volume of material worn (V) is inversely proportional to hardness for a given set of test conditions [12]:

$$V = K \cdot l \cdot \frac{P}{H} \quad (1)$$

where K is the wear coefficient, l is the sliding distance, P is the applied load and H is the hardness.

Nanocrystalline materials generally have a high hardness and are often produced as films; this naturally lends them to coating applications, making their wear properties of great practical importance. Early studies of wear in nanocrystalline metals seem to point to an adherence to the Archard equation [13–16], although very limited data is available for the finest grain sizes (average grain size below ~ 20 nm), where the shift to boundary-dominated deformation occurs and the most pronounced deviations from the Hall–Petch scaling law are observed. To gain a more complete understanding of how the shift to grain boundary-dominated deformation physics affects the wear response of nanocrystalline metals, a systematic study across the full range of grain sizes over which the Hall–Petch breakdown occurs is needed.

* Corresponding author.

E-mail address: schuh@mit.edu (C.A. Schuh).

There are several practical barriers to producing nanocrystalline materials over a wide range of grain sizes, especially spanning the range over which mechanism transitions occur (~ 5 – 50 nm). Many of the common techniques for processing nanocrystalline materials can access only small ranges of grain size or cannot produce sufficient bulk quantities of material for full-scale engineering wear testing [17]. However, electrodeposition can produce nanocrystalline metals with average grain sizes over a very broad range, from the conventional micrometer scale to near the amorphous limit [7,16,18–28]. The Ni–W system is of particular interest, because in this system reverse pulse deposition waveforms can be used to control grain size over a broad range (~ 2 – 200 nm) [29], with all deposits in this range being single phase fcc solid solutions with a small amount of grain boundary segregation that stabilizes the structure [30,31].

Here we report on the wear response of nanocrystalline Ni–W with average grain sizes in the range 3–47 nm using a pin-on-disk testing methodology. Across this range of grain sizes, we explore the influence of microstructure and mechanical properties on wear. While the coarser microstructures appear to follow Archard's equation, a deviation from Archard behavior is found for the finest grain sizes, where grain boundary deformation mechanisms dominate; in these materials, wear resistance is higher than would be expected based on hardness alone. This deviation is traced to a dynamic microstructure in which grain size and grain boundary character evolve under repetitive sliding load, which in turn alters the mechanical response during testing.

2. Materials and methods

Experimental specimens were prepared using the pulsed electrodeposition technique of Detor and Schuh [29], with the same bath chemistry and deposition conditions. Circular steel substrates were prepared for deposition by mechanical polishing, followed by pickling with hydrochloric acid and electrocleaning following ASTM Standard B183-79 [32]. This substrate acted as the cathode during the deposition process, with a platinum mesh anode. The deposited coatings were ~ 50 μm thick, and a range of samples of different grain sizes were produced by tuning the applied current waveform and plating temperature, following Detor and Schuh [29]. After deposition, each sample was mechanically polished to a root mean square roughness of < 20 nm.

Each specimen was characterized by energy dispersive spectroscopy (EDS) in a Leo 438VP scanning electron microscope operated at 20 kV to measure the composition. X-ray diffraction (XRD) profiles were then obtained using a PANalytical X'Pert Pro diffractometer with a Cu $K\alpha$ radiation source operated at 45 kV and 40 mA. The XRD profiles were used to ensure that all specimens were indeed polycrystalline fcc solid solutions and to estimate the average grain size to within $\pm 15\%$ by applying the Scherrer equation [33] to the (1 1 1) peak after subtracting

instrumental broadening. These grain sizes were also verified by transmission electron microscopy (TEM) in bright field imaging mode. Each grain was manually identified and traced, and the equivalent circular diameter was calculated. TEM specimens were prepared using the focused ion beam (FIB) in situ lift-out technique [34] and examined in a JEOL 2010 operated at 200 kV. The measured compositions and grain sizes for the eight different specimens studied here are included in Table 1. We note that in the present alloy system W is a grain refining element, owing to its subtle tendency for grain boundary segregation [30,31]; accordingly, across the samples in Table 1, grain size decreases as W content increases.

Traditional Vickers microhardness was measured using a LECO model LM247 indenter with an applied load of 10 g and a 15 s hold time. Wear tests were carried out with a CSM Instruments pin-on-disk tribometer. Specimens were held in a self-centering chuck and rotated for 10,000 cycles with a constant normal load of 5 N applied 8 mm from the axis of rotation; the total sliding distance for a typical test was therefore about 500 m. A tungsten carbide sphere with a hardness of 22 GPa and 6 mm diameter was used as the counter-body. Three different discrete sliding speeds were used in this work: 0.15, 0.05 and 0.015 m s^{-1} , and the friction coefficient (μ) was measured during each test.

The morphology of the wear tracks was investigated by a combination of scanning electron microscopy (SEM) and surface profilometry using a KLA-Tencor P-16 stylus profiler. SEM imaging allowed for the investigation of wear mechanisms, while profilometry was used to provide a quantitative measurement of wear volume. Due to the irregular surface of the wear track, with a discontinuous transfer layer and numerous peaks and valleys, individual two-dimensional line scans were generally found to be imprecise in characterizing the wear track. In order to improve the statistics of the measurements, three-dimensional scans, such as those shown in Fig. 1a, were carried out at several points on the wear track. These data were then averaged along the wear direction to calculate the representative cross-sectional area of the targeted section of the wear track. An example showing assessment of the representative wear track cross-section is shown in Fig. 1b. On

Table 1
Microstructural and mechanical properties of Ni–W electrodeposits.

W content (at.%)	Average XRD grain size (nm)	Average TEM grain size (nm)	Hardness (GPa)	Wear volume (μm^3)	Friction coefficient
3.0	47		4.0	9.49×10^6	0.63
6.0	30		5.6	7.40×10^6	0.67
8.2	26	25	5.9	5.88×10^6	0.61
12.5	15		6.6	5.12×10^6	0.65
15.7	9		6.8	5.06×10^6	0.66
18.2	6	6	6.9	4.03×10^6	0.65
22.9	5		7.1	3.79×10^6	0.60
27.9	3	3	7.1	2.77×10^6	0.66

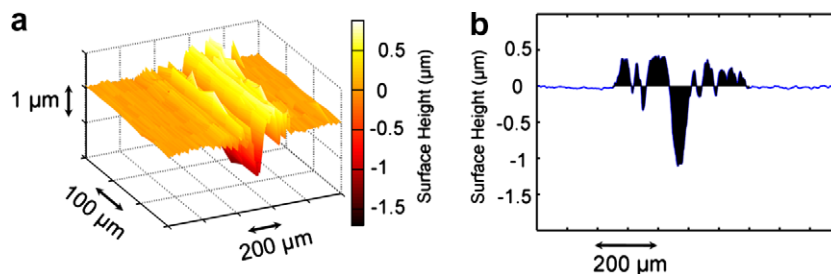


Fig. 1. Surface profiles of a wear scar in a Ni–W specimen. Three-dimensional scans (a) were used to find a representative wear track cross-section (b).

such cross-sections, the area both below and above the initial surface was integrated and multiplied by the track length to determine the total wear volume.

After completion of the wear experiments, characterization of the worn material was also carried out using the various methods described above. Extensive use was made of the FIB lift-out technique to permit TEM observations in the wear track region, including cross-sectional views perpendicular and parallel to the sliding direction.

3. Wear of nanocrystalline Ni–W

Since wear has traditionally been linked to hardness, as for example by Eq. (1), we begin by investigating the relationship between hardness and microstructure in our deposits. Fig. 2 presents hardness as a function of grain size. The hardness measurements are also included in Table 1 and, although it is not shown explicitly here, we find that the present measurements align closely with those reported by Detor and Schuh [29], who used the same processing method to render a similar set of specimens. Our three largest grain sizes (26, 30 and 47 nm) all lie in the range where Hall–Petch scaling is expected:

$$H = H_0 + kd^{-n} \quad (2)$$

where H is the measured hardness, H_0 is the hardness of a single crystal, k is a material constant and d is the average grain size. The Hall–Petch exponent n is usually taken as $1/2$ and, indeed, our three largest grain sizes fit a power law

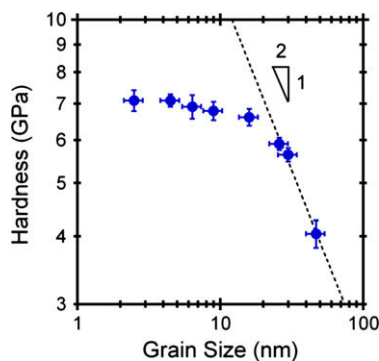


Fig. 2. Hardness of nanocrystalline Ni–W plotted as a function of grain size on double logarithmic scales. The larger grain sizes obey Hall–Petch scaling (exponent of $1/2$, as shown).

with this exponent well, as shown in Fig. 2. At grain sizes of 15 nm and below, we observe the expected breakdown in Hall–Petch scaling. In the Ni–W system, the Hall–Petch breakdown is normally characterized by a plateau in hardness at the finest grain sizes for conventional (low rate) testing [29], whereas a peak and ‘inverse’ Hall–Petch regime are seen primarily at higher deformation rates [35,36]. The activation volumes and energies have also been measured in prior studies on Ni–W across this range of grain sizes, which verified the expected shift from traditional dislocation mechanisms to grain boundary-dominated deformation mechanisms at the finer grain sizes [35,37]. The results in Fig. 2 are in line with these prior studies of the mechanical properties of nanocrystalline Ni–W, and the range of grain sizes covered by the present work spans the mechanistic transition regime.

To systematically study the wear response across this range of grain sizes, pin-on-disk experiments were run at a sliding speed of 0.15 m s^{-1} . In all of our wear tests, the friction coefficient exhibited a transient increase from near zero to a steady-state value after approximately 500 cycles, and then stayed at this value for the remainder of the experiment. The steady-state friction coefficients for all of the specimens fell in the range 0.60–0.67 (Table 1). The similarity of the friction coefficients suggests that all of the specimens wore through the same mechanisms. SEM investigation of the wear tracks confirmed this, with all samples showing evidence of abrasive wear. Fig. 3a and b are typical of results seen on all of the samples, and show top-down SEM views of wear tracks in a sample with a grain size of 26 nm, with the sliding direction denoted by the arrow. In these images, surface plowing by asperities and a flaking and cracked transfer layer can be seen; some patches of the transfer layer are identified by dotted white arrows. EDS and XRD of the wear track showed that the transfer layer was mainly fcc Ni(W) with small amounts of tungsten and nickel oxides. In Fig. 3c, a cross-sectional TEM view revealing the structure of the transfer layer is shown for a specimen with a grain size of 3 nm. In this image the sliding direction is into the page and the dotted white line denotes the true surface of the specimen; the material above the surface is the transfer layer, which is about 500–550 nm thick in this region. Obvious pores and cracks can be seen in the transfer layer, as well as a grain size similar to the as-deposited value. The transfer

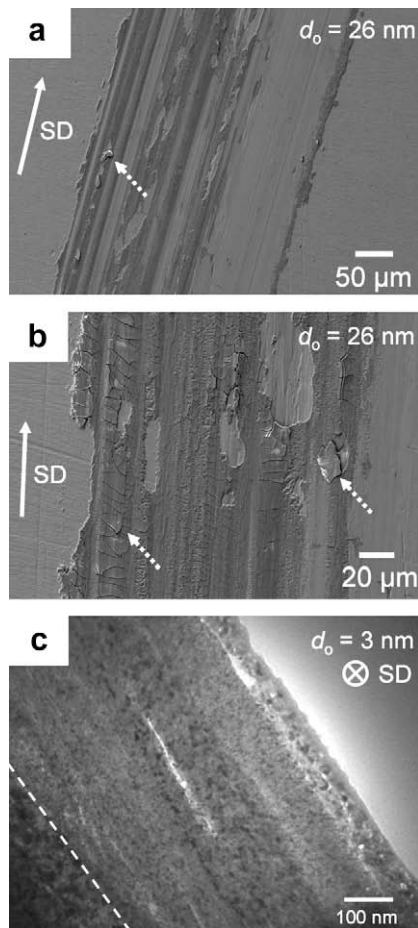


Fig. 3. (a and b) Top-down SEM micrographs of the wear track in a Ni–W sample of 26 nm grain size. Surface plowing by asperities and a flaking, cracked transfer layer (denoted by dotted white arrows) provide evidence of abrasive wear. (c) Cross-sectional bright field TEM image of the transfer layer showing obvious pores, cracks and a grain size unchanged from the as deposited value of 3 nm. The sliding direction (SD) is in the plane of the page in (a) and (b) and into the page in (c). The dashed white line denotes the true surface in (c).

layer also appears to be comprised of a number of discrete layers, suggesting a process of gradual build up over a number of consecutive counter-body traverses.

Fig. 4 presents quantitative measurements of wear in the Ni–W specimens, with wear volume plotted against grain size in Fig. 4a. Table 1 also includes the wear volume measurements. For the entire range of grain sizes studied, wear volume decreased with decreasing grain size, following a consistent trend that is surprisingly well described by a power law with a grain size exponent close to $\frac{1}{2}$. This trend is expected for grain sizes larger than ~ 25 nm, where Hall–Petch hardness scaling is observed, grain refinement leads to significant hardening (H_0 is negligible) and thus the combination of Eqs. (1) and (2) predicts that $V \propto d^{1/2}$. However, it is surprising to see this trend continue into the range of the finest grain sizes below 15 nm, where the hardness plateaus (cf. Fig. 2) and the $\frac{1}{2}$ power law is no longer expected.

The dotted blue¹ line in Fig. 4a shows the expected wear volume based on the Archard equation, i.e. using Eq. (1) with the experimentally measured values for hardness from Fig. 2. If wear volume were in fact inversely proportional to hardness for all of our specimens, a plateau would have been observed in Fig. 4a. The deviation of the data from the dotted line thus suggests that the Archard equation is no longer obeyed at grain sizes below about 10 nm. This is more directly revealed in Fig. 4b, which plots the expected scaling between hardness and wear volume; a linear trend is expected in Fig. 4b according to the Archard equation and for the larger grain sizes the proportionality is well obeyed with a wear constant of $K = 1.53 \times 10^{-5}$. Again, however, the experimental data suggest that the smallest grain sizes wear less than expected.

To investigate the possibility of wear-induced hardening, microhardness measurements were carried out directly on top of the wear tracks. Indentations were made in flat sections of the wear track, with a low load of 10 g being used in order to only probe material near the surface. Special care was taken to avoid placing indentations in the transfer layer, and thus the measurements are reflective of the base material. The typical indentation width in these experiments was ~ 5 μm , much smaller than the width of the wear tracks (150–450 μm), while the depth of the indentations was ~ 700 nm. The hardness measurements from the wear track are presented in Fig. 5, along with measurements from the as-deposited (unworn) material (which are the same as those presented in Fig. 2). The difference between the wear track hardness and as-deposited hardness (ΔH) is plotted against grain size in the inset to Fig. 5, showing that hardening of the wear track becomes more pronounced at the finest grain sizes. Significant hardening (beyond uncertainty) occurred only for grain sizes below about 10 nm.

Taken together, the results in Figs. 4 and 5 suggest that the apparent breakdown of the Archard equation is correlated with wear-induced hardening in the wear track. Both of these phenomena occur at grain sizes below about 10 nm, and become more pronounced at finer grain sizes.

4. Near-surface microstructure

Microstructural changes are often observed near wear surfaces in traditional microcrystalline materials, most commonly in the form of a dislocation substructure [38–40], a mechanically mixed layer [38,41,42] or a nanocrystalline tribolayer [39,41–43]. Such microstructural refinement can result in a hardened surface and is often explained as being caused by frictional heating or highly localized deformation near the surface. However, these concepts do not translate in any straightforward manner to the present nanocrystalline Ni–W specimens. With as-deposited grain

¹ For interpretation of color in Figs. 1, 2, 4, 5, 8–11, the reader is referred to the web version of this article.

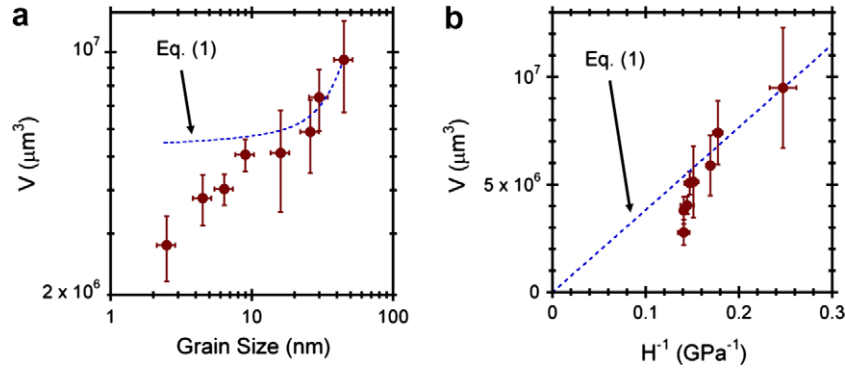


Fig. 4. Quantitative measurements of wear: (a) wear volume plotted against grain size and (b) wear volume plotted against reciprocal hardness. In both (a) and (b) the dotted blue line denotes the expected wear volume based on the Archard equation, given in Eq. (1). The smallest grain sizes (below ~10 nm) wear less than expected.

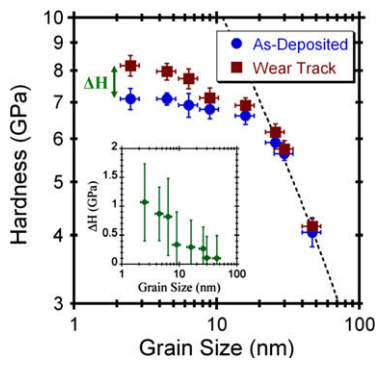


Fig. 5. Hardness measurements from the as-deposited specimens and the wear tracks plotted as a function of grain size. (Inset) The difference between the wear track hardness and the as-deposited hardness (ΔH), showing that hardening of the wear track becomes more pronounced at the finest grain sizes.

sizes as fine as 10 nm or even less, it seems unlikely that wear can cause any further grain refinement, and even if it did, it is unclear how this could account for the hardening observed in Fig. 5, as the Hall–Petch breakdown in Fig. 2 suggests that finer grains are not expected to lead to higher hardness in the range of interest. Accordingly, classical microstructural refinement arguments cannot be applied to the present observations, and direct observations of the worn material microstructure are required.

To investigate the possibility of near-surface microstructural changes in Ni–W during the sliding wear process, TEM lamellae were cut from the wear track using FIB. Fig. 6a shows a top-down view of such a lamella, cut into an unworn surface of a 6 nm grain size specimen; the horizontal ligament in this figure was subsequently removed and imaged in cross-section in the TEM. Fig. 6b shows a

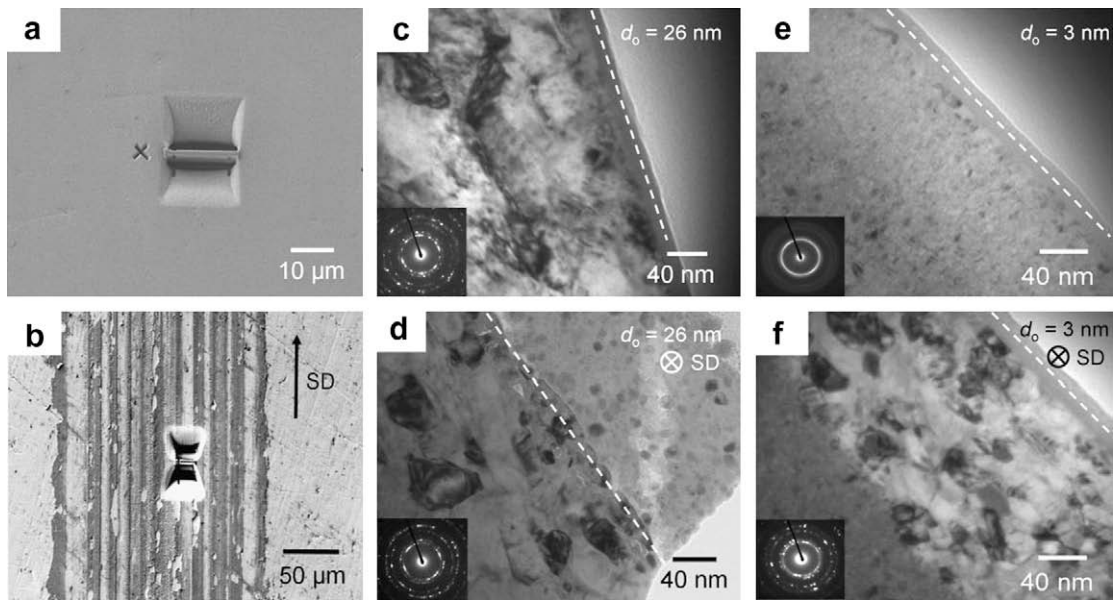


Fig. 6. Top-down SEM views of lamellae cut from (a) an as-deposited specimen and (b) the center of a wear track. Bright field TEM micrographs of the (c) as-deposited and (d) wear track lamellae from the alloy with an initial grain size (d_0) of 25 nm; the dashed white line denotes the surface of the specimen in these cross-sections. Similar cross-sectional bright field TEM micrographs of the (e) as-deposited and (f) wear track lamellae from the alloy with $d_0 = 3$ nm.

similar view of a specimen cut from the center of the wear track. The direct comparison of lamellae from as-deposited (unworn) material and the wear track ensures that any observed microstructural changes subsequently described are not artifacts of the FIB preparation.

First, we examined the alloy with an initial grain size (d_0) of 25 nm, which lies in the range where both Hall–Petch and Archard scaling are followed (cf. Figs. 2 and 4). Bright field cross-sectional TEM micrographs of the as-deposited and wear track samples are presented in Fig. 6c and d. In each image the surface is marked by a dashed white line and the direction of sliding is into the page. Comparison of Fig. 6c and d shows that the wear process led to very little obvious microstructural evolution in this sample. Although a piece of the discontinuous transfer layer can be seen above the surface of the wear specimen in Fig. 6d, the size and shape of the grains beneath the surface is similar to the structure of the as-deposited material in Fig. 6c.

Next, the alloy with an initial grain size of 3 nm, where the most significant deviations from Hall–Petch and Archard scaling were observed (cf. Figs. 2 and 4), was investigated. TEM images of as-deposited and worn material with $d_0 = 3$ nm are presented in Fig. 6e and f, with the surface again marked by a dashed white line and the sliding direction into the page. Comparison of these two images clearly shows a layer with a different microstructure near the surface of the wear track in Fig. 6f. Direct measurements from TEM images show that the average grain size in this layer has increased to ~ 20 nm, from an as-deposited size of 3 nm. Evidence of grain coarsening can also be seen in the selected area diffraction patterns presented in the bottom left of Fig. 6e and f, with the same selected area aperture used for each pattern. The pattern of continuous diffraction rings observed in the as-deposited specimen transitions to one with more discrete spots in the wear specimen. The grain growth layer in the worn specimen is very distinct, sharply separated from the base material beneath, which seems to exhibit the as-deposited structure with an average grain size in the range of just a few nanometers. The thickness of the grain growth layer is found to be in the range 100–300 nm, depending on the location of the measurement; in Fig. 6f the thickness is ~ 160 nm. TEM

lamellae were also taken from the alloy with an initial average grain size of 6 nm to compare the bulk and wear track microstructures. A very similar grain growth layer was observed at the wear surface for this specimen, although TEM images are not included here. In this case, the microstructure coarsened to an average grain size of ~ 25 nm.

To investigate the possibility of anisotropic structural evolution in the grain growth layer, TEM lamellae were also obtained to reveal cross-sections along the sliding direction. Fig. 7a and b show the microstructure at the wear surface from a specimen with $d_0 = 3$ nm when the sliding direction is into the page and in the plane of the page, respectively. No major differences can be seen between the two orientations, although there may be some evidence of shearing in the microstructure in Fig. 7b that is not present in that of Fig. 7a.

It is interesting to note that the grain growth layer we observe in these samples is only ~ 300 nm thick, whereas the hardness measurements used to establish the presence of wear-induced hardening in Fig. 5 involved indentations that were somewhat deeper (700 nm). Accordingly, the data in Fig. 5 underestimate the true hardening in the wear track, as they sample both the grain growth layer and nominally virgin material beneath it. An interesting corollary to this is that the deviation from Archard's law shown in Fig. 4b persists even if the data are plotted against the post-wear hardness values instead of the as-deposited hardness. If clean hardness measurements could be obtained from the very thin ~ 300 nm grain growth layer, we expect that the wear volume may correlate linearly with them. However, even nanoindentation measurements are unreliable at the very fine (~ 30 nm) depths that would be required to probe the grain growth region without any convolution from the virgin material beneath it, so this speculation must remain unproven at present.

5. Discussion

5.1. Relationship between structural evolution and hardening

The above results reveal a consistent picture: at larger grain sizes (above about $d_0 = 10$ nm) wear does not lead

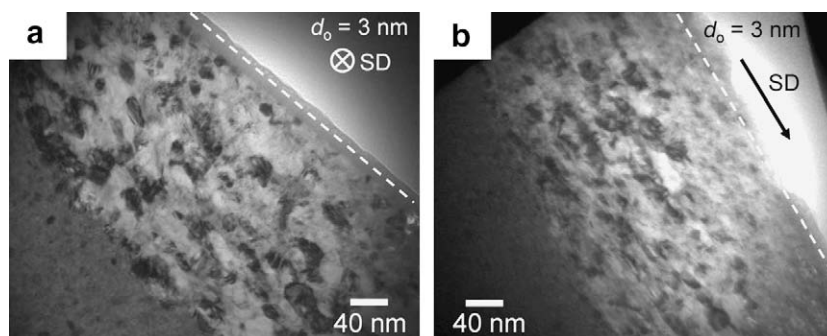


Fig. 7. Cross-sectional bright field TEM micrographs from the wear surface of a specimen with $d_0 = 3$ nm when (a) the sliding direction is into the page and (b) the sliding direction is in the plane of the page.

to substantial changes in the structure of the film, essentially no local hardening is measured in the wear track and the wear properties follow expectations based on the Archard equation. For grain sizes below about 10 nm (as, for example, in the two investigated samples with $d_0 = 3$ and 6 nm) wear induces grain growth, leads to significant surface hardening and, therefore, exhibits the most obvious deviation from Archard scaling.

It is interesting and somewhat counter-intuitive that the wear-induced hardening we see here is associated with grain growth at the surface during the wear process; grain growth is normally associated with softening. This nominally unexpected result is due to the complex nature of structural evolution in a nanocrystalline system that contains a significant alloying addition. As shown in the work of Detor and Schuh [44], under annealing conditions nanocrystalline Ni–W alloys can undergo several concurrent processes of structural change, including grain growth, grain boundary relaxation, precipitation of intermetallic Ni_4W and short-range chemical ordering of W in the fcc solid solution. All of these changes can in principle affect the mechanical properties, and thus the intuitive relationship between grain growth and softening is oversimplified for such alloy systems. In the present case we can rule out several of the above structural changes in the worn material. For example, our TEM and XRD investigations revealed no trace of second phase precipitation of Ni_4W , while analysis of TEM diffraction patterns showed no signature of the chemical short-range ordering which has been observed in annealed Ni–W specimens. In the light of these observations, we would expect that the primary structural evolution processes that occur during wear of Ni–W are grain growth and grain boundary relaxation. Whereas the first of these may cause softening or result in no change in strength (depending on the extent of grain growth), grain boundary relaxation is well established as contributing to hardening in both Ni–W alloys [44] and other nanocrystalline metals [45,46], owing to loss of excess boundary dislocations and reduction of stress concentrations at boundaries.

To develop expectations for the combined effect of grain boundary relaxation and grain growth on hardness in Ni–W, we examine the data of Detor [47], who annealed nanocrystalline Ni–W samples of the same kind as used in this study. From the many different annealing treatments used by Detor, we compile here all of those which involved grain boundary relaxation and grain growth, excluding all of the data that involved intermetallic precipitation. These samples were generally exposed to low temperatures (below 600 °C) for relatively short times (generally less than 24 h and always less than 72 h); full details of the treatments may be found in Detor [47].

The hardness of such annealed specimens is plotted in Fig. 8, along with our measurements on as-deposited specimens. For the sample with an initial grain size of $d_0 = 3$ nm, upon annealing the structure initially hardens due to grain boundary relaxation without any change in

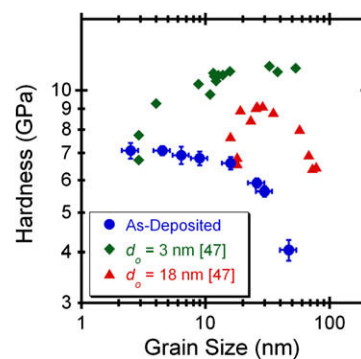


Fig. 8. Hardness as a function of grain size for as-deposited specimens from this study and annealed specimens with $d_0 = 3$ nm and 18 nm from Detor [47].

grain size. Subsequent further annealing leads to grain growth, although the hardness versus grain size relation now follows a curve that is shifted above that for the as-deposited samples. This trend of grain boundary relaxation followed by grain growth is also followed in the annealed sample with an initial grain size of $d_0 = 18$ nm. In both cases we observe that an evolved, coarser microstructure can in fact be harder than an as-deposited, finer microstructure. This provides an important point of validation for our wear results, where wear-induced coarsening and hardening are found to occur together.

Another interesting point shown in Fig. 8 is that for two alloys coarsened to a given final grain size, the material with the smaller initial grain size will be harder. This is probably because the initial materials in this case have different alloying additions; the finer-grained specimens have more tungsten and thus, even when coarsened to the same grain size, have higher strengths due to solution strengthening effects. Such trends are consistent with our observation that the $d_0 = 3$ nm structure hardened more during wear than the $d_0 = 6$ nm structure for coarsening to a similar final grain size, and thus explains why deviations from the Archard law become more severe as grain size is reduced.

A final interesting point that can be taken from the annealing studies of Detor is that the level of coarsening we observe in the worn specimens corresponds to a relatively severe thermal treatment: exposure to 600 °C for more than 3 h would be necessary for grain growth to occur to the extent experienced by our wear specimens (coarsening from 3 to 20 nm) [47]. This observation will motivate the discussion of coarsening mechanisms in the following sections.

5.2. Driving forces for microstructural evolution

As mentioned previously, the most common driving forces for microstructural change during wear are frictional heating and highly localized deformation; in this section we consider these two possibilities in turn, and identify the cause of the structural evolution in our worn samples.

5.2.1. Frictional heating

We first explore surface heating due to friction. The above discussion shows that thermal exposure can certainly lead to the kinds of structural changes and hardening we observe during wear, but it is not clear whether our wear conditions cause sufficient frictional heating to account for such changes. To explore this possibility, we consider the model of Kannel and Barber [48], which is based on one-dimensional transient heat flow analysis, with frictional heating at the contact point and heat removal occurring by conduction into the substrate and convection at the surface; heat loss to the tungsten carbide counter-body is accounted for by using the Blok postulate [49]. Their model is specifically applicable to a pin-on-disk geometry and time-averages the heat transfer over individual cycles. The maximum temperature occurs at the surface, since this is where the heating occurs during sliding contact, and the local surface temperature can be written as:

$$T = \frac{Q_A}{h_s} \left\{ 1 - \operatorname{erfc} \left[h_s \sqrt{\frac{t}{K\rho c}} \right] \exp \left[\frac{h_s^2 t}{K\rho c} \right] \right\} \quad (3)$$

where h_s is the heat transfer coefficient for convection ($\sim 20 \text{ W m}^{-2} \text{ K}^{-1}$ in air), t is the time and K , ρ and c are the thermal conductivity, density and specific heat, respectively, of the substrate material. Q_A is the frictional heating power per unit area and is given by:

$$Q_A = \frac{\mu P v}{A_s} \quad (4)$$

where μ is the friction coefficient, P is the normal load, v is the sliding velocity and A_s is the surface area of the wear track. For our nanocrystalline Ni–W alloys, the thermal conductivity ($94 \text{ W m}^{-1} \text{ K}^{-1}$ [50]) and specific heat ($0.444 \text{ J g}^{-1} \text{ K}^{-1}$ [50]) of Ni are used, while the density is calculated using a rule of mixtures and the densities of Ni (8.9 g cm^{-3} [50]) and W (19.3 g cm^{-3} [50]). The WC counter-body is assigned a thermal conductivity of $84 \text{ W m}^{-1} \text{ K}^{-1}$ [50].

The form of Eq. (3) is such that temperature increases steadily with time, at least in part because conduction is only considered in the direction normal to the surface, ignoring radial heat loss to the substrate. The model thus neglects the evolution to a steady-state condition that is expected in experiments, and it provides upper bound estimates of the achievable temperatures at the surface. For our purposes, and in the spirit of assessing the true upper bound temperature that might be achieved during our experiments, we evaluate the temperature at the end of our tests; a sliding speed of 0.15 m s^{-1} and $t = 3333 \text{ s}$ are used. The output of the model is relatively insensitive to grain size or alloy composition, with only small variations resulting from the different coefficients of friction (Table 1) and densities. Again in the spirit of assessing an upper bound, we report here results using the properties of the alloy with $d_0 = 3 \text{ nm}$, which gives the highest temperatures by a slight margin.

For these conditions, we calculate the upper bound expectation value for local frictional heating in our experiments using Eq. (3) as $\sim 500 \text{ }^\circ\text{C}$. Even if this value is

assumed to hold over the entire duration of a 1 h experiment, the total thermal exposure was low for these alloys; recall our comparison with the thermal annealing study of Detor in the previous section, which suggested a thermal exposure of $600 \text{ }^\circ\text{C}$ for more than 3 h would be required to explain the degree of coarsening seen in these wear experiments. Recognizing that the predicted surface temperature rose gradually, the specimen spends most of the test at temperatures well below $450 \text{ }^\circ\text{C}$, where grain growth is not observed in these alloys [44]. We conclude that the temperature is certainly not high enough for a sufficient period of time to explain the grain growth in our specimens.

We further verify that frictional heating is not responsible for the observed structural evolution in our samples through a set of additional experiments. Specifically, wear tests were run at slower sliding speeds, which results in less frictional heating and leads to lower surface temperatures from Eqs. (3) and (4). Sliding speeds of 0.05 and 0.015 m s^{-1} (respectively one-third and one-tenth the original sliding speed) were used. For these conditions, Eq. (3) provided upper bound surface temperatures of 290 and $160 \text{ }^\circ\text{C}$, respectively. These are well below the temperatures required to induce grain growth in nanocrystalline Ni–W [44].

Wear volume is plotted against grain size for the three different sliding speeds in Fig. 9a. Lowering the sliding speed causes the entire wear volume curve to shift down such that, for a given grain size, less wear damage is observed as the sliding speed decreases. Such behavior is normal in many sliding wear situations, as lower speeds result in lower interface temperatures [49]. It is essential to note that no plateau is observed in the wear volume curve for any given sliding speed; the least wear damage occurs at the smallest grain size for each speed. Thus, the deviation from Archard law behavior (which would lead to a plateau in Fig. 9a) persists at the lower sliding speeds.

To confirm that near-surface microstructure evolution still occurs at slower sliding speeds, where frictional heating effects can be effectively ruled out, TEM specimens from the wear track were taken from the $d_0 = 25$ and 3 nm alloys tested at 0.05 m s^{-1} . For the specimen with $d_0 = 25 \text{ nm}$, like the specimen tested at the original sliding speed, no significant changes are observed in the microstructure near the wear surface. Bright field TEM micrographs of the $d_0 = 3 \text{ nm}$ specimen are presented in Fig. 9c and d, with a similar micrograph taken from the same alloy tested at the original sliding speed (0.15 m s^{-1}) included in Fig. 9b for comparison. Fig. 9c shows a distinct grain growth layer above the bulk microstructure, as well as a fine transfer layer at the surface (which is located above the dashed line). Fig. 9d presents a magnified view of the region denoted by a white box in Fig. 9c, where the coarsened microstructure can be more clearly observed. The thicknesses of the grain growth layer are about the same in the micrographs from the 0.15 and 0.05 m s^{-1} specimens ($\sim 175 \text{ nm}$), although the grain size is slightly higher for

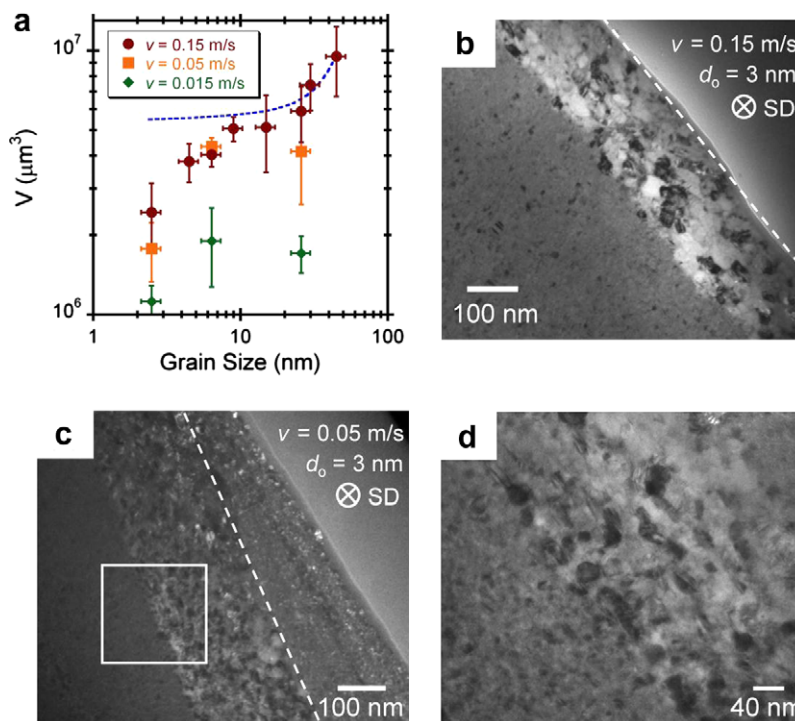


Fig. 9. (a) Wear volume plotted against grain size for three different sliding speeds, showing that the deviation from Archard scaling persists at lower sliding speeds. Bright field TEM micrographs from wear samples with sliding speeds of (b) 0.15 m s^{-1} and (c) 0.05 m s^{-1} show a similar degree of structural change. (d) A magnified view of the region denoted by a white box in (c).

the faster sliding condition. The main point here, however, is that at lower sliding rates where the surface temperature is expected to be sufficiently low that it could not, by itself, cause microstructure coarsening over the timescales of our tests, we still observe a similar degree of structural change after wear. This result, combined with our calculations based on Eq. (3) above, strongly suggests that frictional heating, while it may contribute mildly to coarsening, is not the primary cause of microstructural evolution at the surface during wear.

5.2.2. Deformation-driven structural evolution

The highly localized deformation that occurs at the surface during sliding contact is next considered as a possible cause of microstructural evolution. Recent studies have found evidence of deformation-induced grain growth in pure nanocrystalline metals, such as Al [51,52], Ni [8,53,54], and Cu [55–57], as well as nanocrystalline alloys, such as Ni–Fe [58,59] and Co–P [60]. This grain growth is thought to result from a combination of grain boundary migration and grain rotation caused by the extremely high stresses that develop in a nanocrystalline structure during deformation. Recent results from simulations [9] and experiments [61] have pointed to shear stress in particular as the driving force for such grain growth. In addition, Gianola et al. [51] have shown that deformation-induced grain growth commences during the early stages of plastic deformation and can significantly affect subsequent material response.

To obtain a better understanding of the deformation that occurs near the surface during sliding contact, we consider the stress fields created by a sliding spherical contact. Hamilton [62] provides a set of explicit equations for the subsurface stresses under a sliding spherical contact, assuming only elastic deflections. These equations are only truly rigorous for an idealized geometry and neglect many details of asperity contact, roughness, etc. However, they do permit estimation of the stress fields experienced during wear and identification of the locations where significant plasticity may be expected.

We evaluate the equations of Hamilton using the following inputs: the Young's moduli of Ni (207 GPa [63]) and WC (680 GPa [50]); the Poisson's ratios of Ni (0.31 [63]) and WC (0.24 [50]); the friction coefficient $\mu = 0.66$ (Table 1); the WC counter-body diameter 6 mm. Due to the importance of shear or distortional energy in deformation-induced grain growth [61], the von Mises stress is chosen as the measure of interest. Contour plots of this quantity on a plane through the center of contact with the counter-body are presented in Fig. 10.

Fig. 10a shows the distribution of von Mises stress below the contact for the stationary case, i.e. with only a normal force applied and no sliding. In this limit, the equations reduce to the well-known Hertzian model for sphere on plate contact, with a region of maximum stress below the contact surface at a depth of $\sim 1/2$ the contact radius ($\sim 40 \mu\text{m}$ in the present case). As a tangential force is added in the positive x -direction, the stresses within the material

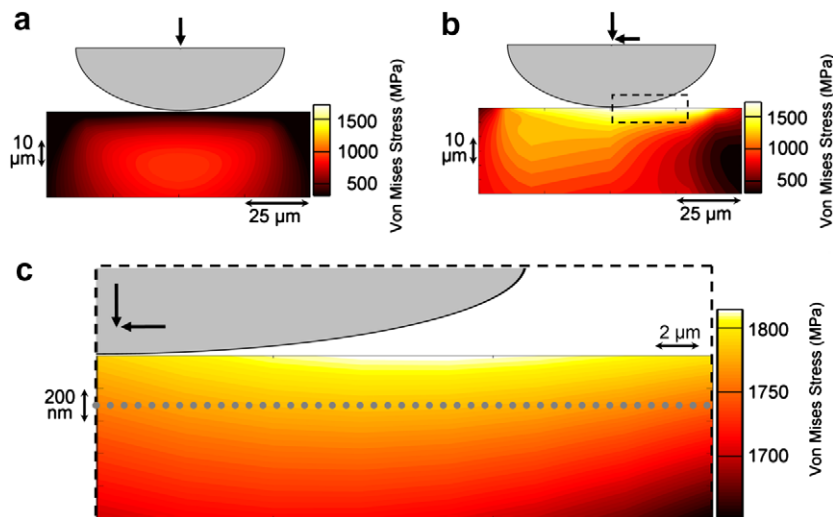


Fig. 10. The distribution of von Mises stress calculated based on elastic contact theory for the cases of (a) only normal loading and (b) normal loading plus sliding. The addition of sliding caused the region of highest stresses to occur at the sliding surface, at the trailing edge of the contact. (c) A magnified view of this region of highest stresses. The dotted gray line denotes the maximum measured thickness of the grain growth layer (300 nm) in our experiments.

increase, the region of maximum stress rises towards the surface and a new region of high stress appears at the trailing edge of the sliding contact. The contours of the von Mises stress beneath the surface for our experimental conditions are presented in Fig. 10b. The relatively high frictional force ($\mu = 0.66$) causes the region of highest stresses to occur at the sliding surface, at the trailing edge of the contact; unlike a normal contact, the subsurface maximum stress region is no longer present.

Fig. 10c presents a magnified view of the stress contours where they are highest; the maximum stress occurs at the contact surface and quickly falls off away from the surface. This provides a first indication that a thin layer of material closest to the surface experiences plasticity in these experiments. A more quantitative argument can be developed by using a modified Tabor relation, $H = 3.8 \sigma_y$, known to apply to nanocrystalline Ni [64], to estimate the yield strength of our specimens. For the range of grain sizes where we observe grain growth in the wear track, the hardness was ~ 6.8 – 7.1 GPa, leading to estimated yield stresses of 1.8–1.9 GPa. Close examination of Fig. 10c reveals that such stress levels are attained primarily within ~ 300 nm of the surface, denoted by a dotted gray line. That the plastic zone expected during wear is of this depth is consistent with the measured thickness of the grain growth regions beneath the wear surface in our samples (which are usually ~ 100 – 300 nm thick; cf. Figs. 6, 7 and 9). This lends support to the notion that the local plasticity caused by sliding contact results in grain growth.

Additional support for a mechanical grain growth mechanism is found through a detailed microscopic examination of the grain growth layer. While the average grain size is significantly increased in the grain growth layer, small grains characteristic of the initial microstructure are still observed. Fig. 11a shows the grain growth layer from

a $d_0 = 3$ nm specimen, where some small grains of < 5 nm diameter are labeled with white arrows. In mechanically-induced grain growth, only select grain boundaries move, resulting in discontinuous (abnormal) growth, which changes the characteristic shape of the grain size distribution. Grain size measurements from the as-deposited material, the wear track and an annealed sample with $d_0 = 3$ nm (3 h at 600 °C) are presented as cumulative distribution plots in Fig. 11b. Both wear and annealing cause grain growth, and a shift in the distributions in Fig. 11b. However, annealing causes a self-similar shift in the distribution, whereas the wear-induced grain growth does not; mean-normalized grain size distributions for the same three specimens are presented in Fig. 11c. The grain size distribution of the worn material has broadened and changed shape, characteristic of abnormal grain growth. This provides further evidence that the grain growth in the wear track is predominantly mechanically-driven, as frictional heating would have led to normal grain growth.

As a final point of discussion, we note that although thermally-driven grain growth is known to be accompanied (or preceded) by grain boundary relaxation [44], the state of grain boundary relaxation after mechanically-driven grain growth remains an open research topic. The present data show that wear induces both grain growth and hardening in nanocrystalline Ni–W, and we view this as primary evidence that mechanical grain growth also involves grain boundary relaxation. We are unaware of significant corroborating data in the literature, although it is interesting to note that molecular dynamics simulations of nanocrystalline Ni [65] show that mechanical deformation causes changes in grain boundary and triple junction structure which resemble those experienced during thermal grain boundary relaxation. In both cases, atomic shuffling and short-range diffusion work to create an equilibrium structure where the

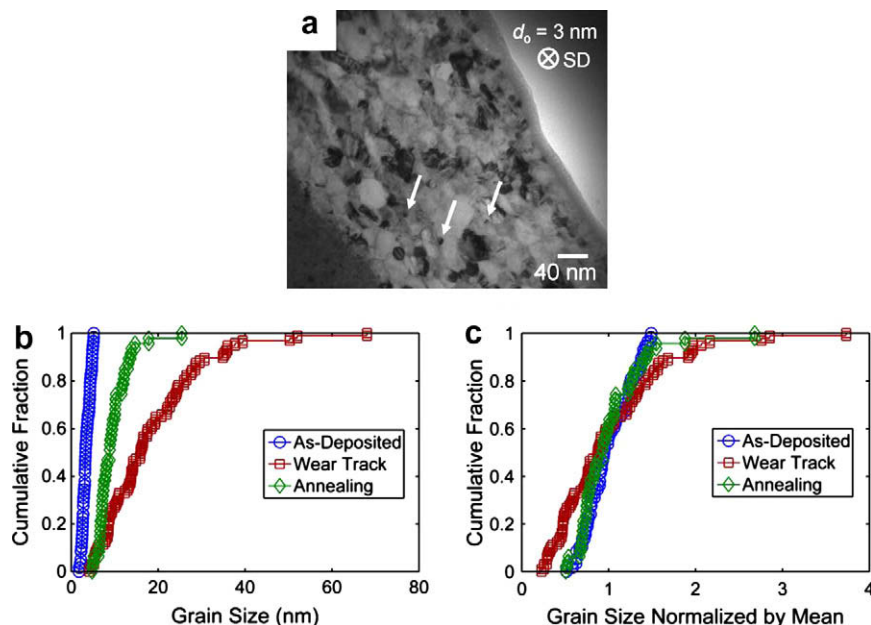


Fig. 11. (a) A bright field TEM micrograph showing the grain growth layer in a $d_0 = 3$ nm wear specimen, with some small grains of < 5 nm diameter labeled with white arrows. Grain size measurements from the as-deposited material, the wear track and an annealed sample with $d_0 = 3$ nm (3 h at 600 °C) are presented as (b) a cumulative distribution plot and (c) a mean-normalized cumulative distribution plot. The grain size distribution from the wear track has broadened in a way characteristic of abnormal grain growth.

number of grain boundary atoms less than 12-coordinated is minimized. With this in mind, it seems likely that the high stresses which cause coarsening near the wear surface may also cause local changes in the atomic boundary structure, resulting in a hardened grain growth layer.

6. Conclusions

The sliding wear of nanocrystalline Ni–W alloys with grain sizes of 3–47 nm was studied experimentally. To our knowledge, the experiments presented here represent the first systematic study of wear in a single nanocrystalline system spanning the entire Hall–Petch breakdown, across which the mechanisms of deformation shift from being intra- to inter-granular. The phenomena observed here provide insight into the superior wear properties of nanocrystalline alloys, which are finding increasing use in tribological applications. The following conclusions can be drawn.

- Nanocrystalline Ni–W alloys exhibit excellent wear properties, with wear resistance continually increasing as grain size decreases. At the finest grain sizes, they wear considerably less than would be expected based upon their as-deposited properties.
- The unexpectedly high wear resistance at grain sizes below 10 nm is traced to significant wear-induced hardening at the surface. Such hardening leads to deviations from the Archard relation, which linearly relates hardness and wear resistance.
- Wear-induced microstructural evolution is observed in the alloys that exhibit significant wear-induced harden-

ing. Specifically, a surface layer with a thickness of a few hundred nanometers exhibits significant grain growth (from, for example, 3 nm to 20 nm). Along with such grain growth, grain boundary relaxation is also expected, and these changes are associated with an increase in hardness after wear. A similar degree of grain growth caused by thermal exposure also leads to hardening of a similar magnitude in these alloys.

- Experiments and calculations suggest that frictional heating is not the main cause of the wear-induced structural evolution we saw in the experiments. On the other hand, the stress state under sliding contact suggests a plastic zone commensurate with the size of the grain growth layer seen in the wear specimens.

These results provide evidence that the grain boundary-dominated mechanisms which control the plastic deformation of nanocrystalline materials can have unexpected consequences under complex loading conditions. Significant microstructural evolution is possible, which can result in a dynamic material response that may change with time in service. That this transient microstructure can, in fact, improve the mechanical properties of the alloy is a fortuitous outcome that may be exploited as nanocrystalline materials become increasingly integrated into mechanical systems.

Acknowledgement

This work was supported by the US Army Research Office under contract W911NF-09-1-0422.

References

- [1] Budrovic Z, Van Swygenhoven H, Derlet PM, Van Petegem S, Schmitt B. *Science* 2004;304:273.
- [2] Chen MW, Ma E, Hemker KJ, Sheng HW, Wang YM, Cheng XM. *Science* 2003;300:1275.
- [3] Cheng S, Spencer JA, Milligan WW. *Acta Mater* 2003;51:4505.
- [4] Schiotz J, Di Tolla FD, Jacobsen KW. *Nature* 1998;391:561.
- [5] Van Swygenhoven H, Derlet PA. *Phys Rev B* 2001;64:9.
- [6] Ke M, Hackney SA, Milligan WW, Aifantis EC. *Nanostruct Mater* 1995;5:689.
- [7] Kumar KS, Suresh S, Chisholm MF, Horton JA, Wang P. *Acta Mater* 2003;51:387.
- [8] Shan ZW, Stach EA, Wiezorek JMK, Knapp JA, Follstaedt DM, Mao SX. *Science* 2004;305:654.
- [9] Cahn JW, Mishin Y, Suzuki A. *Acta Mater* 2006;54:4953.
- [10] Cahn JW, Taylor JE. *Acta Mater* 2004;52:4887.
- [11] Legros M, Gianola DS, Hemker KJ. *Acta Mater* 2008;56:3380.
- [12] Archard JF. *J Appl Phys* 1953;24:981.
- [13] Farhat ZN, Ding Y, Northwood DO, Alpas AT. *Mater Sci Eng A* 1996;206:302.
- [14] Jeong DH, Erb U, Aust KT, Palumbo G. *Scripta Mater* 2003;48:1067.
- [15] Jeong DH, Gonzalez F, Palumbo G, Aust KT, Erb U. *Scripta Mater* 2001;44:493.
- [16] Schuh CA, Nieh TG, Yamasaki T. *Scripta Mater* 2002;46:735.
- [17] Koch CC. *Nanostructured materials: processing, properties, and applications*. Norwich, NY: William Andrew Publishing; 2007.
- [18] Brooks I, Lin P, Palumbo G, Hibbard GD, Erb U. *Mater Sci Eng A* 2008;491:412.
- [19] El-Sherik AM, Erb U. *J Mater Sci* 1995;30:5743.
- [20] Lu K, Wei WD, Wang JT. *Scripta Metall Mater* 1990;24:2319.
- [21] Palumbo G, Erb U, Aust KT. *Scripta Metall Mater* 1990;24:2347.
- [22] Ebrahimi F, Bourne GR, Kelly MS, Matthews TE. *Nanostruct Mater* 1999;11:343.
- [23] Erb U. *Nanostruct Mater* 1995;533.
- [24] Li HQ, Ebrahimi F. *Acta Mater* 2003;51:3905.
- [25] Schuh CA, Nieh TG, Iwasaki H. *Acta Mater* 2003;51:431.
- [26] Wu BYC, Ferreira PJ, Schuh CA. *Metall Mater Trans A* 2005;36A:1927.
- [27] Lu L, Sui ML, Lu K. *Science* 2000;287:1463.
- [28] Iwasaki H, Higashi K, Nieh TG. *Nanomater Struct Appl* 2003;740:119.
- [29] Detor AJ, Schuh CA. *Acta Mater* 2007;55:371.
- [30] Detor AJ, Miller MK, Schuh CA. *Phil Mag* 2006;86:4459.
- [31] Detor AJ, Miller MK, Schuh CA. *Phil Mag Lett* 2007;87:581.
- [32] ASTM. *Standard B183-79*. West Conshohocken, PA: ASTM International; 2009.
- [33] Cullity BD. *Elements of X-ray diffraction*. Reading, MA: Addison-Wesley; 1959. p. 262.
- [34] Giannuzzi LA, Stevie FA. *Introduction to focused ion beams: instrumentation, theory, techniques, and practice*. New York: Springer; 2005.
- [35] Trelewicz JR, Schuh CA. *Acta Mater* 2007;55:5948.
- [36] Trelewicz JR, Schuh CA. *Appl Phys Lett* 2008;93:3.
- [37] Trelewicz JR, Schuh CA. *Scripta Mater* 2009;61:1056.
- [38] Hughes DA, Dawson DB, Korellis JS, Weingarten LI. *J Mater Eng Perform* 1994;3:459.
- [39] Rigney DA, Chen LH, Naylor MGS, Rosenfield AR. *Wear* 1984;100:195.
- [40] Rigney DA, Glaeser WA. *Wear* 1978;46:241.
- [41] Singh JB, Cai W, Bellon P. *Wear* 2007;263:830.
- [42] Singh JB, Wen JG, Bellon P. *Acta Mater* 2008;56:3053.
- [43] Emge A, Karthikeyan S, Rigney DA. *Wear* 2009;267:562.
- [44] Detor AJ, Schuh CA. *J Mater Res* 2007;22:3233.
- [45] Volpp T, Goring E, Kuschke WM, Arzt E. *Nanostruct Mater* 1997;8:855.
- [46] Weertman JR. *Mater Sci Eng A* 1993;166:161.
- [47] Detor AJ. PhD thesis, Department of Materials Science and Engineering, Massachusetts Institute of Technology, Cambridge, MA; 2007.
- [48] Kannel JW, Barber SA. *Tribol Trans* 1989;32:305.
- [49] Bhushan B. *Modern tribology handbook*. Boca Raton, FL: CRC Press; 2001.
- [50] Shackelford JF, Alexander W, Park JS. *CRC materials science and engineering handbook*. Boca Raton (FL): CRC Press; 1994.
- [51] Gianola DS, Van Petegem S, Legros M, Brandstetter S, Van Swygenhoven H, Hemker KJ. *Acta Mater* 2006;54:2253.
- [52] Jin M, Minor AM, Stach EA, Morris JW. *Acta Mater* 2004;52:5381.
- [53] Pan D, Nieh TG, Chen MW. *Appl Phys Lett* 2006;88:3.
- [54] Wang YB, Li BQ, Sui ML, Mao SX. *Appl Phys Lett* 2008;92:3.
- [55] Brandstetter S, Zhang K, Escudero A, Weertman JR, Van Swygenhoven H. *Scripta Mater* 2008;58:61.
- [56] Zhang K, Weertman JR, Eastman JA. *Appl. Phys. Lett.* 2004;85:5197.
- [57] Zhang K, Weertman JR, Eastman JA. *Appl Phys Lett* 2005;87:3.
- [58] Fan GJ, Wang YD, Fu LF, Choo H, Liaw PK, Ren Y, et al. *Appl Phys Lett* 2006;88:3.
- [59] Wang YB, Ho JC, Liao XZ, Li HQ, Ringer SP, Zhu YT. *Appl Phys Lett* 2009;94:3.
- [60] Fan GJ, Fu LF, Qiao DC, Choo H, Liaw PK, Browning ND. *Scripta Mater* 2006;54:2137.
- [61] Rupert TJ, Gianola DS, Gan Y, Hemker KJ. *Science* 2009;326:1686.
- [62] Hamilton GM. *J Mech Eng Sci* 1983;197:53.
- [63] American Society for Metals. *Metals handbook. Properties and selection: nonferrous alloys and pure metals, vol. 2*. Metals Park, OH: American Society for Metals; 1989.
- [64] Dalla Torre F, Van Swygenhoven H, Victoria M. *Acta Mater* 2002;50:3957.
- [65] Hasnaoui A, Van Swygenhoven H, Derlet PM. *Acta Mater* 2002;50:3927.